

# Automatic Map Density Selection for Locally-Performant Visual Place Recognition

Somayah Hussaini, Tobias Fischer, Michael Milford  
QUT Centre for Robotics, Queensland University of Technology, Australia  
{s.hussaini, tobias.fischer, michael.milford}@qut.edu.au

**Abstract**—A key challenge in translating Visual Place Recognition (VPR) from the lab to long-term deployment is ensuring a priori that a system can meet user-specified performance requirements across different parts of an environment, rather than just on average globally. A critical mechanism for controlling local VPR performance is the density of the reference mapping database, yet this factor is largely neglected in existing work, where benchmark datasets with fixed, engineering-driven (sensors, storage, GPS frequency) sampling densities are typically used. In this paper, we propose a dynamic VPR mapping approach that uses pairs of reference traverses from the target environment to automatically select an appropriate map density to satisfy two user-defined requirements: (1) a target Local Recall@1 level, and (2) the proportion of the operational environment over which this requirement must be met or exceeded, which we term the Recall Achievement Rate (RAR). Our approach is based on the hypothesis that match patterns between multiple reference traverses, evaluated across different map densities, can be modelled to predict the density required to meet these performance targets on unseen deployment data. Through extensive experiments across multiple VPR methods and the Nordland and Oxford RobotCar benchmarks, we show that our system consistently achieves or exceeds the specified local recall level over at least the user-specified proportion of the environment. Comparisons with alternative baselines demonstrate that our approach reliably selects the correct operating point in map density, avoiding unnecessary over-densification. Finally, ablation studies and analysis evaluate sensitivity to reference map choice and local space definitions, and reveal that conventional global Recall@1 is a poor predictor of the often more operationally meaningful RAR metric.

## I. INTRODUCTION

Visual place recognition (VPR) is the task of identifying whether a given query place has been previously visited by finding its match within a large set of previously visited places, commonly referred to as the reference database [20, 24, 35, 12]. The VPR field, both as stand alone research and as components of SLAM and Visual Localization systems, has been an increasingly active area of research in recent years, with highly capable systems built on modern machine learning pipelines capable of superb performance on research benchmark datasets [24, 35]. But excellent performance on benchmark datasets using research metrics like global recall@1 do not necessarily translate into useful systems in practice. One key example of this is the need to achieve a certain R@1 performance on a *local* basis in each section of the environment - a performance metric we call the Recall Achievement Rate (RAR). **RAR is poorly predicted by global R@1 performance** - the same global recall average

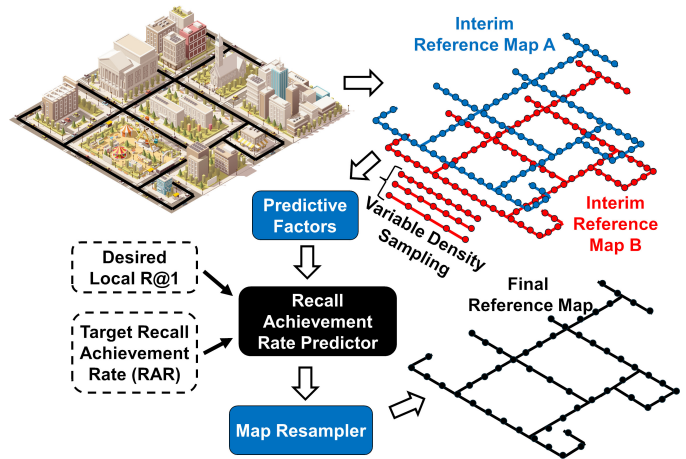


Fig. 1: Our approach models the relationship between local Recall@1 performance and factors extracted from analysis of variable density sampling of initial map data, in order to produce a final map density that ensures a user-specified local Recall@1 performance requirement is met or exceeded for a user-required percentage of local regions of the environment, dubbed the Recall Achievement Rate (RAR).

can be achieved by every part of the environment achieving that same recall rate, or by half of the environment achieving a very high recall rate and the other performing dismally (as we show in this work). Then there is the additional challenge of needing to determine the configuration that will achieve this required performance *ahead of time*, rather than in a retrospective performance analysis as is typical in research papers.

To address these challenges, in this paper we present a dynamic VPR mapping approach that models the relationship between variable density sampling of two reference traverses from the operating environment and recall rates to automatically select the appropriate VPR map density to use in subsequent VPR (Figure 1). Our approach enables users to specify two key performance requirements: 1) a Local Recall@1 threshold (e.g., 10% or 90%) that is desired to be achieved in a local part of the environment, and 2) the percentage of the operational environment (on a locale/segment basis that is defined by a fixed physical distance) for which that threshold must be met or exceeded, which we call the Recall Achievement Rate (RAR). We demonstrate our system consistently being able to achieve a wide range of user-specified

RARs over the complete range of target Recall@1 rates, and across multiple VPR methods and benchmark datasets, without making the reference map denser than it needs to be. We also present ablations and analysis that evaluate the sensitivity of the method to the locale definition - how big a local region is considered to be - as well as to the ordering of the reference traverses, and results that starkly demonstrate the huge disconnect between what is normally reported on: global R@1 averages - and the RAR.

## II. RELATED WORK

This section provides an overview of visual place recognition and its recent developments, followed by density sampling techniques used in SLAM and the wider robot navigation domain, and finally covers reference database refinement techniques in the VPR domain. While adaptive sampling has been explored in SLAM for keyframe selection, and VPR research has investigated reference database manipulation for improved performance, to the best of our knowledge, the study of selecting an appropriate *reference density* to meet specific requirements remains unexplored in the VPR domain. Our work bridges this gap by introducing a dynamic VPR mapping approach to automatically determine appropriate reference density sampling rates that satisfy user-defined local Recall@1 and Recall Achievement Rate (RAR) targets.

### A. Visual place recognition

In visual place recognition approaches, reference and query images are typically converted into compact feature representations to better enable a query image to match its corresponding reference image, despite potential changes in appearance and viewpoint [20, 24, 35, 12]. Early VPR methods relied on hand-crafted features such as FAB-MAP [11], Bag of Words (BoW) [29], and VLAD [16]. The field evolved significantly with CNN-based approaches such as NetVLAD [4], which demonstrated superior robustness to appearance and viewpoint variations.

More recent and current state-of-the-art VPR methods leverage diverse strategies. These strategies include the use of novel spatial pooling and aggregation techniques such as Generalised Mean Pooling (GeM) [27] and Conv-AP [1]. Other strategies include the use of loss functions tailored for the VPR domain [28, 19] and novel training strategies and architectures. MixVPR [2] combines CNN backbones and Feature Mixer layers to form global relationships between feature maps. CosPlace [6] transforms VPR training into a classification task by arranging data into distinct geographical classes.

Other works use Vision Transformers to improve VPR robustness, including SALAD [15], which uses the concept of the optimal transport problem for descriptor aggregation; AnyLoc [17], which uses the DinoV2 foundation model without any fine-tuning for VPR; CricaVPR [21], which incorporates awareness of cross-image correlation; BoQ [3], which performs cross-attention and aggregates information via learnable global queries; and Megaloc [5], which fuses

data from multiple datasets and leverages best practices from related fields to VPR to improve robustness. All these VPR methods focus primarily on improving *descriptor quality* to handle appearance changes. However, most VPR systems are demonstrated using a densely sampled reference database and optimise for global Recall@1 performance. However, they do not consider how local recall rates vary spatially and how reference density affects these local performance guarantees, which is the focus of our work.

### B. Sampling techniques in SLAM and robot navigation

In SLAM and visual odometry systems, keyframe selection directly impacts computational efficiency and system robustness. Traditional approaches select keyframes at fixed distance or time intervals, but this uniform strategy presents a fundamental trade-off: dense sampling incurs high computational overhead, while sparse sampling risks missing critical loop closures.

To address this, several adaptive keyframe selection strategies have been proposed in the SLAM domain. Piao and Kim [26] introduced an adaptive keyframe selection approach using IMU data for motion estimation. Chen et al. [10] introduced an approach which involves creating submaps using a variant density sampling sliding window and merging those submaps to obtain a consistent map. Zu et al. [36] used statistical analysis of inter-frame pose differences combined with a fuzzy inference mechanism to dynamically adjust keyframe selection thresholds based on camera motion uncertainty and complexity. In the LiDAR-SLAM domain, Chen et al. [9] sampled keyframes based on the environment spaciousness, and Zeng et al. [34] used information theory to determine when to create a new keyframe, both of which require manual tuning. More recently, Stathoulopoulos et al. [30] introduced the Minimal Subset Approach (MSA), which uses sliding window combinatorial optimisation to minimise keyframe redundancy while preserving essential information for both place recognition and pose graph optimisation components of LiDAR SLAM. Thorne et al. [32] introduced a neural network-based point cloud descriptors with submodular optimisation to adaptively select unique keyframes and generate submaps that maximise localisation constraints while minimising memory usage for LiDAR SLAM.

While these SLAM-based works show the value of adaptive sampling, they typically focus on varying local keyframe density based on motion dynamics and map consistency. Our work addresses the challenge of selecting a uniform spatial reference density for database construction in VPR to determine the sparsest global reference density that satisfies user-specified local performance targets. This represents a complementary but distinct problem: SLAM methods optimise *where* to sample densely, while we determine *what uniform sampling rate* ensures that user-specific requirements are met.

### C. Reference database refinement methods for VPR

Several VPR works have explored the strategic manipulation of reference databases to enhance VPR performance, although

with different objectives than our work here.

Yin et al. [33] introduced MRS-VPR, which uses a coarse-to-fine retrieval pipeline with multi-resolution down-sampling of reference images, where particle filtering is used to refine candidate matches from sparse to dense resolutions, balancing computational efficiency and match accuracy. Lee and Hwang [18] proposed Bag of Sampled Words, a sampling-based strategy for local descriptor selection to improve robustness in changing environments, focusing on which features to sample within images rather than which images to include. Molloy et al. [25] introduced Bayesian Selective Fusion, which selects and fuses informative reference images to improve matching accuracy, prioritising information content over storage efficiency. Malone et al. [23] followed a similar approach of prioritising information content by fusing reference images from multiple reference sets recorded under different conditions to improve match accuracy.

These approaches primarily aim to improve matching robustness and/or retrieval speed by selecting informative reference images or features, some of which operate at query time. In contrast, our work focuses on reducing storage requirements through adaptive spatial density sampling determined at map construction time, based on the intrinsic per-segment characteristics of the environment. Rather than selecting the most informative individual images, we learn to determine the appropriate reference sampling density for entire spatial segments, enabling storage reduction while maintaining performance across diverse environments.

### III. METHODOLOGY

In this work, we study how changes in reference density sampling affect the performance of visual place recognition (VPR) models both locally and globally, where each segment (a local region) is defined over a fixed physical distance. We investigate how selecting an appropriate reference density sampling rate can ensure that user-specified local performance requirements are met and reduce the number of reference images for storage.

To achieve this goal, we propose an automatic reference density sampling selector that analyses VPR performance characteristics at the segment level to inform the selection of a single sampling density for the entire operational environment at query time. Given user-specified target local recall@1 and target recall achievement rate (RAR) thresholds, our approach selects the sparsest sampling rate that meets or exceeds these requirements. Our approach leverages two reference traversals (Ref1, Ref2) to predict per-segment recall@1 performance and use these predictions to select the optimal sampling rate offline, which is then applied uniformly across all segments and evaluated at query time with an independent query traversal.

Our automatic selector method is agnostic to the underlying VPR approach, making it generalisable to any VPR model. This generalisability ensures that our methodology can be applied across different VPR systems without requiring VPR model-specific modifications.

#### A. Problem formulation

We assume that the VPR dataset consists of repeated traversals corresponding to a robot traversing a path. Our setup includes two reference traversals (Ref1 and Ref2) and one query traversal (Qry1), all covering the same route with a one-to-one spatial correspondence between frames. Qry1 is held out entirely and used only for final evaluation.

We split each reference traversal into  $N$  segments, denoted  $S = \{s_1, s_2, \dots, s_i, \dots, s_N\}$ , where each segment  $s_i$  covers approximately  $d$  meters of physical distance.

We denote the set of  $M$  reference density sampling rates as follows:

$$\mathcal{K} = \{k_1, k_2, k_3, \dots, k_M\}, \quad (1)$$

where  $k \in \mathcal{K}$  indicates sampling every  $k$ -th reference frame (e.g.,  $k = 1$  uses all frames,  $k = 2$  uses every other frame). Query sampling is fixed at  $k = 1$  (every frame) to ensure comprehensive coverage.

#### B. Reference density sampling selector process

Using the setup defined above, our pipeline, as shown in Figure 2, proceeds as follows:

##### Phase 1: Model training and sampling rate selection using (Ref1, Ref2)

- 1) For each reference density sampling rate  $k \in \mathcal{K}$ , we compute distance scores between Ref1 and Ref2 using the base VPR model at that sampling rate.
- 2) For each segment  $s_i$  in the entire (Ref1, Ref2) traversal at each sampling rate  $k$ , we extract  $F_{i,k}$  features from the distance matrix and compute the segment’s ground truth recall at 1 as the target output.
- 3) We train one Ridge regression predictor for each sampling rate  $k$  using all segments from (Ref1, Ref2) to learn from the full diversity of the route’s characteristics.
- 4) For all segments of (Ref1, Ref2) at each sampling rate  $k$ , we apply the corresponding trained predictor to predict recall@1 ( $\hat{R}_{i,k}$ ) for a given segment  $s_i$  based on its extracted features  $F_{i,k}$ . Note that while these are the same segments used for training, the predictions serve only to inform sampling rate selection and are not used as performance metrics.
- 5) For each sampling rate  $k$ , we count the number of segments whose predicted recall@1 meets or exceeds the user-specified per-segment target recall@1 threshold to compute the predicted recall achievement rate (RAR).
- 6) The selector chooses the sparsest sampling rate  $k^*$  whose predicted RAR meets or exceeds the user-specified target RAR threshold.
- 7) We curate a reference database, Ref1\*, by applying the selected sampling rate  $k^*$  uniformly to the Ref1 traversal.

While training and selecting on the same (Ref1, Ref2) data could introduce bias, this is mitigated by: (i) Ridge regression’s L2 regularisation, (ii) the simple model with only  $F$  features, and (iii) final evaluation on the completely independent (Ref1\*, Qry1) pair with unseen query data. We describe the details of these steps in the following subsections.

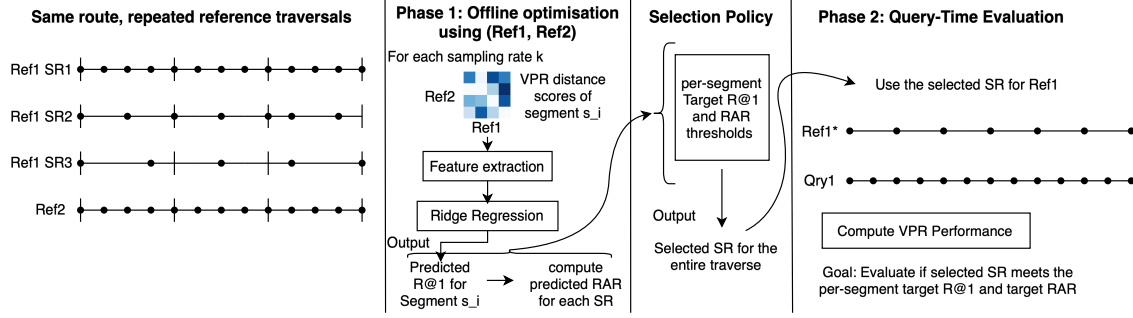


Fig. 2: Overview of our automatic reference density selection framework. (A) Input reference traversals are segmented and processed at varying densities. (B) Features extracted from the (Ref1, Ref2) similarity matrix are used to train density-specific Ridge regressors that predict segment-wise Recall@1. (C) The selection policy identifies the sparsest sampling rate that satisfies the user-defined target recall achievement rate (RAR). (D) The optimised reference map is generated and evaluated against the unseen query traversal (Qry1).

### C. Feature extraction for the recall@1 predictor

For each segment  $s_i$  at the sampling rate  $k$ , we extract  $F = 4$  features from the VPR distance matrix that capture the spatial structure and quality of place matches. Within each segment, we retrieve the top-1 predicted reference index for each query image, and obtain its corresponding spatial position  $p_{i,j}$  for  $j = 1, \dots, n_{q,i}$ , where  $n_{q,i}$  is the number of query images within segment  $s_i$  (from Ref2 traversal). We define the feature vector  $\mathbf{x}_{i,k} = [x_{i,k,1}, x_{i,k,2}, x_{i,k,3}, x_{i,k,4}]^T$  as follows:

1) *Jump Rate* ( $x_{i,k,1}$ ): Measures the fraction of consecutive query predictions within the segment with large spatial discontinuities:

$$x_{i,k,1} = \frac{1}{n_{q,i} - 1} \sum_{j=1}^{n_{q,i}-1} \mathbb{1} [|p_{i,j+1} - p_{i,j}| > \tau], \quad (2)$$

where  $\tau$  is a distance tolerance threshold (ground-truth tolerance in meters) and  $\mathbb{1}[\cdot]$  is the indicator function. High jump rates suggest inconsistent place matching.

2) *Fraction Outside Main Cluster* ( $x_{i,k,2}$ ): Captures the proportion of predictions falling outside the dominant spatial region within the segment. We discretise prediction positions into spatial bins of width  $d$  meters (matching the segment distance), identify the most frequent bin, and compute:

$$x_{i,k,2} = 1 - \frac{1}{n_{q,i}} \sum_{j=1}^{n_{q,i}} \mathbb{1} [b_{i,j} \in \{b_i^* - 1, b_i^*, b_i^* + 1\}], \quad (3)$$

where  $b_{i,j} = \lfloor p_{i,j}/d \rfloor$  is the bin index for prediction  $j$  in segment  $s_i$  and  $b_i^*$  is the most frequent bin in segment  $s_i$ . Higher values indicate spatially scattered predictions.

3) *Largest Cluster Fraction* ( $x_{i,k,3}$ ): Measures the proportion of predictions in the segment that belong to the largest spatially coherent cluster within the segment:

$$x_{i,k,3} = \frac{\max_c |C_{i,c}|}{n_{q,i}}, \quad (4)$$

where  $C_{i,c}$  denotes a cluster of predictions with consecutive spatial positions within the ground-truth tolerance  $\tau$  in segment  $s_i$ , and  $|C_{i,c}|$  is the cluster size. Clusters are formed by sorting prediction positions and identifying breaks where consecutive positions differ by more than  $\tau$ . A high largest

cluster fraction indicates that most predictions are spatially concentrated, suggesting consistent place matching.

4) *Turn Rate* ( $x_{i,k,4}$ ): Quantifies non-monotonic behaviour in the prediction sequence of the segment using the second-order difference:

$$x_{i,k,4} = \frac{1}{n_{q,i} - 2} \sum_{j=1}^{n_{q,i}-2} \mathbb{1} [(p_{i,j+2} - 2p_{i,j+1} + p_{i,j}) \neq 0]. \quad (5)$$

A high turn rate indicates frequent changes in the direction of predicted positions, suggesting matching instability.

We compute these features for the reference-to-reference pair (Ref1, Ref2) during the offline phase. These features are designed to capture matching consistency and spatial coherence.

### D. Segment-wise recall at 1 predictor

We use Ridge regression (L2-regularised linear regression) as our predictor to predict per-segment recall at 1. We use this model for its robustness to multicollinearity and its ability to prevent overfitting and to generalise well, even when the feature space is moderate relative to the number of training samples.

For each sampling rate  $k$ , the Ridge regression model is defined as:

$$f_k(\mathbf{x}_{i,k}) = \mathbf{w}_k^T \mathbf{x}_{i,k} + b_k, \quad (6)$$

where  $\mathbf{w}_k \in \mathbb{R}^F$  is the weight vector and  $b_k \in \mathbb{R}$  is the bias term for sampling rate  $k$ . The model parameters are learned by minimising the regularised least squares objective:

$$\mathbf{w}_k^*, b_k^* = \arg \min_{\mathbf{w}_k, b_k} \sum_{i=1}^N (R_{i,k} - \mathbf{w}_k^T \mathbf{x}_{i,k} - b_k)^2 + \lambda \|\mathbf{w}_k\|_2^2, \quad (7)$$

where  $N$  is the total number of segments,  $R_{i,k}$  is the ground truth recall@1 for segment  $s_i$  at sampling rate  $k$  on (Ref1, Ref2), and  $\lambda$  is the regularisation parameter that controls the trade-off between fitting the training data and model complexity.

The predictor output  $\hat{R}_{i,k} = f_k(\mathbf{x}_{i,k})$  represents the predicted recall@1 for segment  $s_i$  at sampling rate  $k$ .

### E. Sampling rate selection policy

The predictor outputs per-segment recall@1 estimates  $\hat{R}_{i,k}$  for each sampling rate  $k$ . The selector then uses these predictions to choose a single sampling rate for the entire traversal that meets user-specified performance requirements while minimising reference storage.

Given user-specified requirements, a per-segment target recall@1 ( $R_{\text{target}}$ ) and a target recall achievement rate ( $\text{RAR}_{\text{target}}$ ), the selection proceeds as follows:

1) *Computing the predicted recall achievement rate (RAR)*: For each sampling rate  $k$ , we compute the predicted recall achievement rate by counting the fraction of segments whose predicted recall@1 meets or exceeds the per-segment target recall@1. This is defined as follows:

$$\widehat{\text{RAR}}_k = \frac{1}{N} \sum_{i=1}^N \mathbb{1} [\hat{R}_{i,k} \geq R_{\text{target}}], \quad (8)$$

where  $N$  is the total number of segments and  $\mathbb{1}[\cdot]$  is the indicator function.

2) *Selecting the sampling rate*: The selector finds all feasible sampling rates whose predicted RAR meets or exceeds the target RAR threshold, then selects the sparsest among them to minimise storage. If no sampling rate achieves the target RAR, the selector falls back to the sampling rate with the highest predicted RAR. We define this as follows:

$$k^* = \begin{cases} \max\{k \in \mathcal{K} : \widehat{\text{RAR}}_k \geq \text{RAR}_{\text{target}}\} & \text{if feasible} \\ \arg \max_{k \in \mathcal{K}} \widehat{\text{RAR}}_k & \text{otherwise} \end{cases} \quad (9)$$

where ‘‘if feasible’’ means  $\exists k \in \mathcal{K} : \widehat{\text{RAR}}_k \geq \text{RAR}_{\text{target}}$ , and  $\max\{k \in \mathcal{K}\}$  selects the largest  $k$  (corresponding to the sparsest sampling rate) among feasible candidate density sampling rates.

The selected sampling rate  $k^*$  is then applied uniformly across all segments to construct the reference database Ref1\* for query-time evaluation.

## IV. EXPERIMENTAL SETUP

### A. Implementation details

#### Phase 2: Query-time Evaluation using (Ref1\*, Qry1)

At query time, for each query image in Qry1, we compute distances to the reference database Ref1\* (constructed using the selected sampling rate  $k^*$ ) and calculate recall at 1. This provides the final evaluation of how well the chosen reference density sampling rate meets the specified operating conditions on truly unseen query data.

This approach answers the key question: If we run a VPR system twice along the same route (Ref1, Ref2) and determine the most suitable sampling rate using predicted performance, how well does this chosen sampling rate meet the user-specified requirements on per-segment target recall@1 and target RAR when applied at query time (Ref1\*, Qry1)? Critically, the query data (Qry1) is never used during the training or selection process.

### B. Datasets

1) *Nordland dataset*: This dataset [31] captures a 728 km train journey in Norway recorded across four seasons. Following standard practice [13, 8], we remove segments where train speed falls below 15 km/h using the provided GPS data. We use the fall and spring traverses as Ref1 and Ref2, and the summer traverse as Qry1. We use the first 20,000 images with segment distance  $d = 200$  m resulting in 100 segments. We assume each image is approximately 1m apart, and we use a ground truth tolerance of  $\pm 50$  m.

2) *Oxford RobotCar dataset*: This dataset [22] contains over 100 traverses of Oxford city captured under varying conditions including different times of day and seasons. Following prior works [25, 14], we use front-left stereo frames from the Sun (2015-08-12-15-04-18) and Rain (2015-10-29-12-18-17) traverses as Ref1 and Ref2, and the Dusk (2014-11-21-16-07-03) traverse as Qry1. We sample the images approximately once per meter resulting in 3,800 places per traverse. With segment distance  $d = 50$  m, this results in 61 segments. We use a ground truth tolerance of  $\pm 25$  m.

### C. Backbone VPR models

We evaluate our approach using the following VPR methods, MixVPR [2] and Cosplace [6]. We use the implementation of these VPR methods available within the VPR method evaluation repository [7].

### D. Reference density sampling rates

For Ref1, we evaluate the following reference density sampling rates:  $k = \{1, 2, 3, 4, 5, 10, 15, 20, 25, 30, 35, 40, 45, 50\}$ . Ref2 and Qry1 sampling rates are maintained at full density ( $k = 1$ ).

### E. Baselines

1) *Fixed static baseline*: is a fixed sampling rate ( $k=4$ ) that is chosen to operate across all operating conditions, as well as across the evaluated VPR models and datasets.

### F. Performance metrics

1) *Recall Achievement Rate (RAR)*: To evaluate the effectiveness of the per-segment selection policy, we introduce the Recall Achievement Rate (RAR), which measures the proportion of segments where the achieved recall at 1 meets or exceeds the target recall at 1:

$$\text{RAR} = \frac{1}{N} \sum_{i=1}^N \mathbb{1} [R_{i,k} \geq R_{\text{target}}], \quad (10)$$

where  $N$  is the total number of segments,  $R_{i,k}$  is the ground truth recall@1 for segment  $s_i$  using the selected sampling rate  $k^*$ , and  $R_{\text{target}}$  is the target recall at 1.

During Phase 1 (selection), we compute RAR using predicted recalls ( $R_{i,k} = \hat{R}_{i,k}$ ) from our Ridge regression predictor on (Ref1, Ref2) to guide the selection of appropriate density sampling  $k^*$ . During Phase 2 (evaluation), we compute RAR using ground truth recalls ( $R_{i,k} = R_{i,k^*}$ ) on the unseen query data (Ref1\*, Qry1) to assess the actual performance

of the selected sampling rate. This metric enables direct comparison between our approach and a fixed baseline across all configurations. A higher RAR indicates that more segments meet the target recall at 1.

## V. RESULTS

### A. Automatic reference density sampling selector performance at query time

This section evaluates the performance of our approach at query time. We demonstrate that our approach reliably meets or exceeds user-specified target RAR thresholds for the complete range of local R@1 targets (from 0.2 to 1.0) across different VPR methods and datasets, whereas a fixed constant sampling rate across all configurations fails to provide consistent performance guarantees.

Table I presents the deviation from the achievable RAR to the achieved RAR across a range of target R@1 and RAR threshold combinations for all evaluated VPR methods and datasets. The achievable RAR is the RAR of a sampling density which is above the target RAR. Our method adaptively selects different sampling rates depending on the target RAR threshold. The heatmaps for our approach show that the values are greater than or equal to zero (ranging from white to progressively darker shades of blue), indicating that the target RAR is achieved across these VPR methods and datasets tested. Positive values represent cases where our method exceeds the target by a margin. Among all acceptable sampling rates that meet the target RAR, our method favours sparser sampling densities, reducing storage requirements without sacrificing performance guarantees.

The heatmaps in the right-hand columns are for a static baseline approach where the same constant sampling rate (SR=4) is used for these different VPR methods and datasets. These heatmaps of the baseline method contain several negative values (shaded in red), indicating failure to achieve the required RAR. This baseline struggles particularly at high per-segment target R@1 and high target RAR regions. For example, MixVPR on Nordland at target R@1 = 100% shows a deficit of -0.64 across all RAR thresholds. Furthermore, the behaviour of this fixed baseline is dataset-dependent: SR4 mostly succeeds on Oxford RobotCar but fails drastically on Nordland for both MixVPR (at target R@1 = 100%, and marginally at target R@1 = 80% and 60%) and CosPlace (at target R@1 = 80% and 100% and marginally at target R@1 = 60% and 40%, especially at higher target RARs). Using a constant sampling rate across all configurations results in high variability in the achieved RAR (ranging from -0.64 to +0.80 relative to the target as seen in the baseline columns). Our approach provides substantially more consistent outcomes (ranging from 0 to +0.70 above the target), ensuring reliable performance guarantees critical for real-world deployment.

Table II provides a comparison of the mean absolute deviation (MAD) between the achievable and achieved RAR scores to summarise the overall consistency of our approach compared to the baseline across all tested configurations. Our approach consistently achieves significantly lower MAD

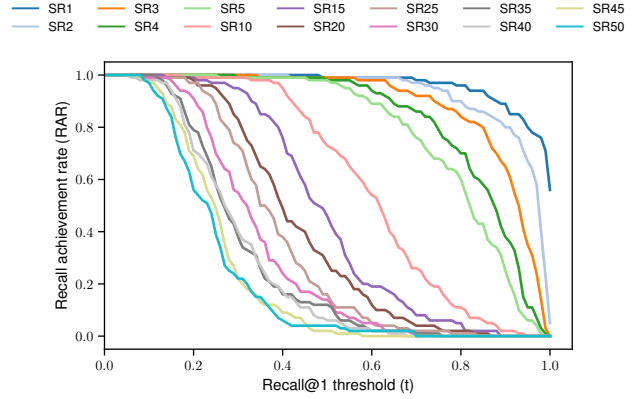


Fig. 3: The recall at 1 performance of the different reference density sampling rates (from dense (SR1:  $k=1$ ) to sparsest (SR50:  $k=50$ )) on a per-segment basis from Cosplace on Nordland against the recall achievement rates, which is the percentage of segments whose per-segment R@1 is equal to or greater than the R@1 threshold ( $t$ ).

values, ranging from 0.07 to 0.10, while the fixed baseline obtains much higher deviations, ranging from 0.12 to 0.36. This substantial reduction in MAD across the evaluated VPR methods and datasets demonstrates that our approach provides more stable and predictable performance guarantees compared to the fixed baseline.

Figure 4 shows a qualitative example of how our approach adjusts the reference density sampling to satisfy different user requirements. For a moderate requirement (target R@1 60%, target RAR 40%), our approach selects a sparse sampling rate ( $k=15$ ), which provides sufficient reference density sampling to meet the requirements. Conversely, as the user increases the performance constraints (target R@1 80%, target RAR 60%), our approach selects a denser sampling rate ( $k=5$ ) to ensure that the more stringent local recall targets are met. Our results show that our approach performs successfully across the evaluated VPR methods and datasets. This supports our hypothesis that reference-to-reference matching patterns are predictive of query-time deployment performance, enabling automatic density selection that reliably meets user-specified local performance requirements.

### B. Segment-wise impact of reference density sampling on VPR performance

This section analyses how reference density sampling affects VPR performance at both global and local levels. Understanding this relationship is important for our automatic selector, which leverages these reference density sampling rates to choose appropriate densities for user-specified requirements.

Global trends: On average and as might be intuitively expected, denser sampling rates achieve higher mean R@1, with performance decreasing as density sampling becomes sparser.

Per-segment observations: The cumulative distribution plots in Figure 3 from CosPlace on Nordland show more nuanced behaviour at the segment level. The fraction of segments

TABLE I: RAR deviation between achieved vs achievable RAR. **Red** indicates missing the max achievable/target. A white cell indicates achieving the exact target, whilst progressively more **Blue** cells indicate exceeding it (with consequent extra frames and map density). Success Rate counts how many targets were met per row. **Bold** indicates the best success rate.

(a) Nordland - MixVPR													
Target RAR		Ours					Baseline					Success Rate	
		0.2	0.4	0.6	0.8	1.0	0.2	0.4	0.6	0.8	1.0	Ours	Base
Target R@1	0.2	0.00	0.00	0.00	0.07	-0.01	0.37	0.37	0.37	0.20	0.00	4/5	5/5
	0.4	0.12	0.15	0.23	0.14	0.00	0.80	0.55	0.40	0.17	0.00	5/5	5/5
	0.6	0.07	0.00	0.31	0.00	0.00	0.77	0.32	0.32	0.01	-0.03	5/5	4/5
	0.8	0.48	0.00	0.00	0.06	0.00	0.63	0.15	0.15	0.00	-0.15	5/5	4/5
	1.0	0.00	0.00	0.00	0.00	0.00	-0.64	-0.64	-0.64	-0.64	-0.64	5/5	0/5

(b) Nordland - CosPlace													
Target RAR		Ours					Baseline					Success Rate	
		0.2	0.4	0.6	0.8	1.0	0.2	0.4	0.6	0.8	1.0	Ours	Base
Target R@1	0.2	0.00	0.13	0.22	0.06	-0.01	0.44	0.44	0.31	0.09	0.00	4/5	5/5
	0.4	0.14	0.27	0.19	0.04	0.00	0.75	0.50	0.23	0.04	-0.01	5/5	4/5
	0.6	0.00	0.35	0.00	0.09	0.00	0.40	0.40	0.05	0.05	-0.05	5/5	4/5
	0.8	0.00	0.10	0.24	0.12	0.00	0.10	0.10	0.10	-0.14	-0.26	5/5	3/5
	1.0	0.00	0.00	0.00	0.00	0.00	-0.56	-0.56	-0.56	-0.56	-0.56	5/5	0/5

(c) Oxford RobotCar - MixVPR													
Target RAR		Ours					Baseline					Success Rate	
		0.2	0.4	0.6	0.8	1.0	0.2	0.4	0.6	0.8	1.0	Ours	Base
Target R@1	0.2	0.00	0.00	0.00	0.00	0.00	0.00	0.00	0.00	0.00	0.00	5/5	5/5
	0.4	0.00	0.00	0.00	0.00	0.00	0.00	0.00	0.00	0.00	0.00	5/5	5/5
	0.6	0.00	0.00	0.00	0.00	0.00	0.08	0.08	0.08	0.08	0.00	5/5	5/5
	0.8	0.00	0.00	0.00	0.00	0.00	0.41	0.41	0.21	0.11	0.00	5/5	5/5
	1.0	0.70	0.47	0.33	0.13	0.00	0.70	0.47	0.33	0.13	0.00	5/5	5/5

(d) Oxford RobotCar - CosPlace													
Target RAR		Ours					Baseline					Success Rate	
		0.2	0.4	0.6	0.8	1.0	0.2	0.4	0.6	0.8	1.0	Ours	Base
Target R@1	0.2	0.01	0.01	0.01	0.01	0.00	0.01	0.01	0.01	0.01	0.00	5/5	5/5
	0.4	0.00	0.00	0.00	0.00	0.00	0.01	0.01	0.01	0.01	0.00	5/5	5/5
	0.6	0.00	0.00	0.11	0.09	0.00	0.21	0.21	0.21	0.11	0.00	5/5	5/5
	0.8	0.17	0.17	0.09	0.16	0.00	0.51	0.51	0.34	0.16	0.00	5/5	5/5
	1.0	0.68	0.54	0.32	0.12	0.00	0.64	0.50	0.28	0.08	-0.04	5/5	4/5

TABLE II: Comparison of Mean Absolute Deviation (MAD) of RAR scores against target thresholds across all target R@1 and target RAR thresholds. Lower is better.

Datasets	VPR methods	Ours	Baseline (SR4)
Nordland	MixVPR	0.0656	0.3584
	CosPlace	0.0784	0.2904
Oxford RobotCar	MixVPR	0.0653	0.1232
	CosPlace	0.1000	0.1563

achieving a given per-segment R@1 threshold varies substantially across sampling rates. The curves are fairly spaced apart, which indicates that sampling density has a pronounced impact on per-segment performance.

Ground-truth tolerance impact: The R@1 performance of all sampling rates is influenced by ground-truth tolerance. Modern VPR systems are generally tolerant of slight viewpoint changes, enabling them to match queries to nearby reference places. With a relatively high ground-truth tolerance (e.g.,  $\pm 50m$ ), even sparse sampling rates maintain a reasonable R@1 relative to denser ones. For instance, for MixVPR on Nordland,  $k=50$  achieves a mean R@1 of 26% compared to 98% obtained by a dense sampling rate  $k=1$  (a difference of 72 percentage points) while using only 2% of the reference images (400 vs. 20000). A tighter tolerance would lower absolute R@1 across all rates, but their relative differences remain fairly similar.

Our results show that the impact of the sampling rate varies by dataset, VPR method, and local segment difficulty. Selecting an appropriate single sampling density for an entire dataset is therefore non-trivial: a rate that works well for one configuration may fail for another. Our automatic selector addresses this by choosing the sparsest sampling density, which is applied uniformly across all segments, that still meets the user-specified local performance requirements.

### C. Correlation between R@1 vs RAR performance metrics

Figure 5 demonstrates that **a high global R@1 does not guarantee a high RAR for a given target**. For example, for a per-segment target R@1 of 100%, the  $k=3$  density sampling achieves a mean R@1 of 91.94% but a RAR of only 1%. Despite the global metric suggesting near-perfect performance, only 1% of segments actually meet the 100% local recall

requirement. This demonstrates that mean R@1 can mask critical local performance failures.

RAR is dependent on the per-segment target R@1 threshold, whereas the mean R@1 does not. The same sampling rate achieves vastly different RAR values depending on the per-segment target R@1 threshold, while its mean R@1 remains fixed. As the target threshold increases, the RAR curve shifts leftward, meaning that fewer segments meet the stricter requirement, while the mean R@1 stays constant. Consequently, the correlation between these two metrics changes with the target R@1 requirement: they may appear related at low thresholds but diverge substantially at high thresholds.

The RAR captures where recall is achieved across the operational environment, whereas mean R@1 only measures how much recall is achieved overall. Two sampling rates with similar mean R@1 can have different RAR values, meaning equal global performance does not translate to equal deployment readiness. This validates the need for RAR as a complementary metric when local performance guarantees are required.

### D. Ablation study on swapping the role of the two reference sets

We performed an experiment where we swapped the roles of the two reference sets. In the original setting, predictors are trained on (Ref1, Ref2) and evaluated on (Ref1\*, Qry1), while in the swapped setting, training uses (Ref2, Ref1) and evaluation uses (Ref2\*, Qry1). This evaluates whether performance depends on the specific reference traverse used for training.

Across most operating conditions, the original and swapped configurations show identical or negligible deviation from the target RAR, indicating that the method generalises well to different reference traverses. Larger differences are observed only at per-segment target R@1 values (0.2 and 0.8), where the swapped configuration increases RAR by up to 0.24. This experiment showed that our method learns generalisable spatial matching characteristics.

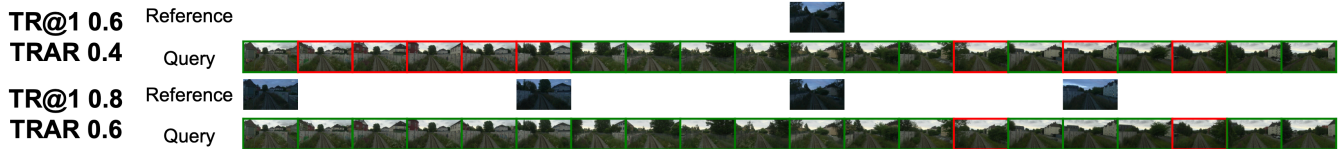


Fig. 4: Qualitative results: given the user-specified conditions, our approach selects a reference density sampling rate that meets the conditions using sparse sampling density. [Top] For a target R@1 of 60% and a target RAR of 40%, the segment’s achieved R@1 is 60% using our approach with a sampling rate of 15. [Bottom] For a target R@1 of 80% and a target RAR of 60%, the segment’s achieved R@1 is 90% with a sampling rate of 5.

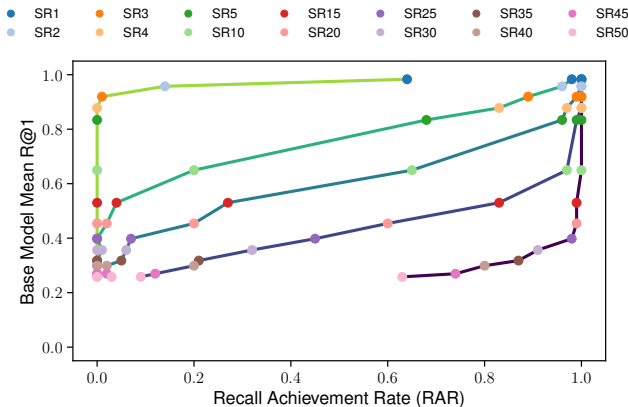


Fig. 5: The recall achievement rate (RAR) of the different sampling rates against the mean R@1 for different per-segment target R@1 of 20%, 40%, 60%, 80% and 100% from MixVPR on Nordland. Observations: the RAR metric is dependent on the per-segment target R@1 whereas the global mean R@1 is not. With increasing per-segment target R@1, the point for the same sampling density is pushed leftward, as less segments meet that stricter target R@1.

#### E. Ablation study on the impact of changing the segment length

We performed an experiment on changing the segment length  $d$  from 50m to 300m in steps of 50m to analyse how segment length affects our approach’s ability to capture local spatial matching characteristics and achieve target RAR across different per-segment target R@1 conditions.

Across most operating conditions, all segment length variations achieve perfect target matching (zero deviation from target RAR), particularly for target R@1 values of 0.4-0.6 and RAR thresholds between 60-100%. Shorter segment lengths (50-100m) occasionally show larger positive deviations under some conditions (e.g., target R@1 = 1.0 with target RAR=20%) with deviations reaching up to 0.61. Longer segment lengths (250-300m) show more conservative and stable behaviour, with near-zero deviation across a wide range of conditions. Minor under-achievement (up to -0.11) occurs at low target R@1 and high RAR, which might be due to difficult regions being averaged out within longer segments. Overall, segment lengths in the 150-200m range maintain stable performance with sufficient capability to adapt to local variations.

## VI. LIMITATIONS

This section describes the limitations of our approach. Our approach uses independent Ridge regression models for each sampling rate, which provides high interpretability and low computational overhead. However, they may fail to capture more complex nonlinear patterns in highly challenging settings. Our approach assumes that the two reference sets and the query set all have one-to-one correspondence. This is a reasonable assumption in a range of scenarios where a robot is tasked with repeatedly navigating a particular environment, such as a warehouse robot. We acknowledge that by using sparser reference density sampling rates, we incur a loss of precision as the number of ground-truth matching reference places for a given query image reduces. To ensure that every query image has at least one ground-truth reference image, we increased our ground-truth tolerance to be equal to the segment length, trading-off localisation accuracy for higher recall reliability.

## VII. FUTURE WORK

Whilst the work demonstrated here provides users with a means by which to ensure a certain recall performance level is achieved across a certain percentage of the deployment environment, there are a range of exciting areas for further enhancement and generality. Firstly, we have focused here on a key VPR and localization relevant metric - Recall@1 for each local segment of the environment - but other functionally-relevant metrics could also be easily targeted, such as worst case performance or ”mean / median/ maximum Euclidean or angular error. Likewise, while the current system provides the user with the ability to specify their desired RAR in the aggregate across the dataset, this could also be done in a *spatially specific* manner: for example, biasing the system to prioritise hitting the local target R@1 rate in specific locations where performance is particularly critical (like a pedestrian crossing or a navigational decision point). Here, the mechanism by which we achieved the user performance requirements was varying the density of the reference map, but this could also be achieved in other ways, such as by varying the fidelity and number of sensor snapshots obtained in each location. Additionally, the loss of spatial precision caused by sparse sampling can potentially be mitigated by interpolating the queries’ position between sparse reference frames. Pragmatically, a number of future improvements are likely feasible: system parameters such as segment size and reference map

density are likely dependent and can be optimized together, and more than two reference sets can be used for calibration.

#### ACKNOWLEDGMENTS

This research was partially supported by funding from ARC Laureate Fellowship FL210100156 to MM and ARC DECRA Fellowship DE240100149 to TF. The authors acknowledge continued support from the Queensland University of Technology (QUT) through the Centre for Robotics.

#### REFERENCES

- [1] Amar Ali-bey, Brahim Chaib-draa, and Philippe Giguere. Gsv-cities: Toward appropriate supervised visual place recognition. *Neurocomputing*, 513:194–203, 2022.
- [2] Amar Ali-Bey, Brahim Chaib-Draa, and Philippe Giguere. Mixvpr: Feature mixing for visual place recognition. In *Proceedings of the IEEE/CVF winter conference on applications of computer vision*, pages 2998–3007, 2023.
- [3] Amar Ali-Bey, Brahim Chaib-draa, and Philippe Giguere. BoQ: A place is worth a bag of learnable queries. In *Proceedings of the IEEE/CVF Conference on Computer Vision and Pattern Recognition*, pages 17794–17803, 2024.
- [4] Relja Arandjelovic, Petr Gronat, Akihiko Torii, Tomas Pajdla, and Josef Sivic. NetVLAD: CNN Architecture for Weakly Supervised Place Recognition. *IEEE Transactions on Pattern Analysis and Machine Intelligence*, 40(6):1437–1451, 2018.
- [5] Gabriele Berton and Carlo Masone. Megaloc: One retrieval to place them all. In *Proceedings of the Computer Vision and Pattern Recognition Conference*, pages 2861–2867, 2025.
- [6] Gabriele Berton, Carlo Masone, and Barbara Caputo. Rethinking visual geo-localization for large-scale applications. In *Proceedings of the IEEE/CVF Conference on Computer Vision and Pattern Recognition*, pages 4878–4888, 2022.
- [7] Gabriele Berton, Gabriele Trivigno, Barbara Caputo, and Carlo Masone. Eigenplaces: Training viewpoint robust models for visual place recognition. In *Proceedings of the IEEE/CVF International Conference on Computer Vision*, pages 11080–11090, 2023.
- [8] Luis G Camara and Libor Přeučil. Visual place recognition by spatial matching of high-level CNN features. *Robotics and Autonomous Systems*, 133:103625, 2020.
- [9] Kenny Chen, Brett T Lopez, Ali-akbar Aghamohammadi, and Ankur Mehta. Direct lidar odometry: Fast localization with dense point clouds. *IEEE Robotics and Automation Letters*, 7(2):2000–2007, 2022.
- [10] Weinan Chen, Changfei Fu, Lei Zhu, Shing-Yan Loo, and Hong Zhang. Ruminations meets VSLAM: You do not need to build all the submaps in realtime. *IEEE Transactions on Industrial Electronics*, 71(8):9212–9221, 2023.
- [11] Mark Cummins and Paul Newman. FAB-MAP: Probabilistic localization and mapping in the space of appearance. *The International journal of robotics research*, 27(6):647–665, 2008.
- [12] Sourav Garg, Tobias Fischer, and Michael Milford. Where Is Your Place, Visual Place Recognition? In *International Joint Conference on Artificial Intelligence*, pages 4416–4425, 2021.
- [13] Stephen Hausler, Sourav Garg, Ming Xu, Michael Milford, and Tobias Fischer. Patch-netvlad: Multi-scale fusion of locally-global descriptors for place recognition. In *Proceedings of the IEEE/CVF conference on computer vision and pattern recognition*, pages 14141–14152, 2021.
- [14] Somayeh Hussaini, Michael Milford, and Tobias Fischer. Spiking neural networks for visual place recognition via weighted neuronal assignments. *IEEE Robotics and Automation Letters*, 7(2):4094–4101, 2022.
- [15] Sergio Izquierdo and Javier Civera. Optimal transport aggregation for visual place recognition. In *Proceedings of the IEEE/CVF conference on computer vision and pattern recognition*, pages 17658–17668, 2024.
- [16] Hervé Jégou, Matthijs Douze, Cordelia Schmid, and Patrick Pérez. Aggregating local descriptors into a compact image representation. In *IEEE/CVF Conference on Computer Vision and Pattern Recognition*, pages 3304–3311, 2010.
- [17] Nikhil Keetha, Avneesh Mishra, Jay Karhade, Krishna Murthy Jatavallabhula, Sebastian Scherer, Madhava Krishna, and Sourav Garg. Anyloc: Towards universal visual place recognition. *IEEE Robotics and Automation Letters*, 9(2):1286–1293, 2023.
- [18] Sang Jun Lee and Sung Soo Hwang. Bag of sampled words: a sampling-based strategy for fast and accurate visual place recognition in changing environments. *International Journal of Control, Automation and Systems*, 17(10):2597–2609, 2019.
- [19] María Leyva-Vallina, Nicola Strisciuglio, and Nicolai Petkov. Data-efficient large scale place recognition with graded similarity supervision. In *Proceedings of the IEEE/CVF Conference on Computer Vision and Pattern Recognition*, pages 23487–23496, 2023.
- [20] Stephanie Lowry, Niko Sünderhauf, Paul Newman, John J Leonard, David Cox, Peter Corke, and Michael J Milford. Visual place recognition: A survey. *IEEE Transactions on Robotics*, 32(1):1–19, 2015. ISSN 1552-3098.
- [21] Feng Lu, Xiangyuan Lan, Lijun Zhang, Dongmei Jiang, Yaowei Wang, and Chun Yuan. Cricavpr: Cross-image correlation-aware representation learning for visual place recognition. In *Proceedings of the IEEE/CVF Conference on Computer Vision and Pattern Recognition*, pages 16772–16782, 2024.
- [22] Will Maddern, Geoffrey Pascoe, Chris Linegar, and Paul Newman. 1 year, 1000 km: The oxford robotcar dataset. *The International Journal of Robotics Research*, 36(1):

- 3–15, 2017.
- [23] Connor Malone, Somayeh Hussaini, Tobias Fischer, and Michael Milford. A hyperdimensional one place signature to represent them all: Stackable descriptors for visual place recognition. In *Proceedings of the IEEE/CVF International Conference on Computer Vision*, pages 9822–9833, 2025.
- [24] Carlo Masone and Barbara Caputo. A survey on deep visual place recognition. *IEEE Access*, 9:19516–19547, 2021.
- [25] Timothy L Molloy, Tobias Fischer, Michael Milford, and Girish N Nair. Intelligent reference curation for visual place recognition via Bayesian selective fusion. *IEEE Robotics and Automation Letters*, 6(2):588–595, 2020.
- [26] Jin-Chun Piao and Shin-Dug Kim. Real-time visual-inertial SLAM based on adaptive keyframe selection for mobile AR applications. *IEEE Transactions on Multimedia*, 21(11):2827–2836, 2019.
- [27] Filip Radenović, Giorgos Tolias, and Ondřej Chum. Fine-tuning CNN image retrieval with no human annotation. *IEEE transactions on pattern analysis and machine intelligence*, 41(7):1655–1668, 2018.
- [28] Jerome Revaud, Jon Almazán, Rafael S Rezende, and Cesar Roberto de Souza. Learning with average precision: Training image retrieval with a listwise loss. In *Proceedings of the IEEE/CVF International Conference on Computer Vision*, pages 5107–5116, 2019.
- [29] Sivic and Zisserman. Video Google: A text retrieval approach to object matching in videos. In *Proceedings ninth IEEE international conference on computer vision*, pages 1470–1477. IEEE, 2003.
- [30] Nikolaos Stathoulopoulos, Christoforos Kanellakis, and George Nikolakopoulos. A Minimal Subset Approach for Informed Keyframe Sampling in Large-Scale SLAM. *IEEE Robotics and Automation Letters*, 11(1):738–745, 2026.
- [31] Niko Sünderhauf, Peer Neubert, and Peter Protzel. Are we there yet? Challenging SeqSLAM on a 3000 km journey across all four seasons. In *Proc. of workshop on long-term autonomy, IEEE international conference on robotics and automation (ICRA)*, page 2013. Citeseer, 2013.
- [32] David Thorne, Nathan Chan, Yanlong Ma, Christa S Robison, Philip R Osteen, and Brett T Lopez. Submodular optimization for keyframe selection & usage in slam. In *2025 IEEE International Conference on Robotics and Automation (ICRA)*, pages 5033–5039. IEEE, 2025.
- [33] Peng Yin, Rangaprasad Arun Srivatsan, Yin Chen, Xueqian Li, Hongda Zhang, Lingyun Xu, Lu Li, Zhenzhong Jia, Jianmin Ji, and Yuqing He. Mrs-vpr: a multi-resolution sampling based global visual place recognition method. In *2019 International conference on robotics and automation (ICRA)*, pages 7137–7142. IEEE, 2019.
- [34] Qihua Zeng, Dong Liu, Yang Zhou, and Yaxin Peng. Entropy-based Keyframe Established and Accelerated Fast LiDAR Odometry and Mapping. In *2023 IEEE 7th Information Technology and Mechatronics Engineering Conference (ITOEC)*, volume 7, pages 347–354. IEEE, 2023.
- [35] Xiwu Zhang, Lei Wang, and Yan Su. Visual place recognition: A survey from deep learning perspective. *Pattern Recognit.*, 113:107760, 2021.
- [36] Linan Zu, Chengrui Wei, Qiqi Sun, Mingyue Zhang, Ning Sheng, and Shuzhi Sam Ge. Adaptive keyframe selection strategy of visual SLAM in complex poses. *IEEE Sensors Journal*, 2024.

# Automatic Map Density Selection for Locally-Performant Visual Place Recognition

## Supplementary Material

### S1. OVERVIEW

This supplementary material extends the experimental analysis presented in the main manuscript, providing deeper insights across six key areas: the design rationale for the hand-crafted predictor features; the distribution of deviations between achieved and achievable recall achievement rate (RAR); analysis of the RAR and reference density relationship under two conditions: varying target RAR at a fixed target R@1, and varying target R@1 at a fixed target RAR; evidence that global mean recall can obscure local recall variability; and visualisations supporting ablation studies on reference set role swapping and segment length variation.

It is important to emphasise that this is an attempt to provide an intuitive explanation of these system components and why they are promising: the hard evidence of their functionality is provided by the standard quantitative evaluations across methods and datasets provided in the main body of work. Firstly, we provide our design rationale behind the hand-crafted features of the predictor in Section S1-A. We then present comprehensive performance analyses: the distribution of the RAR deviations across VPR models and datasets in Section S1-B, the trade-offs between recall achievement rate (RAR) and reference density in Section S1-C, and extend results on how the global mean recall can mask local recall variability in Section S1-D. Finally, we provide supporting visualisations for the two ablation studies introduced in the main manuscript: swapping the roles of the two reference sets in Section S1-E and varying the segment length in Section S1-F. Collectively, we hope that this material provides additional detail about many of the interesting characteristics and phenomenon of the proposed system, and answers some of the natural questions that might arise beyond those already addressed in the main manuscript.

#### A. Design rationale behind the hand-crafted features of the predictor

In this section, we provide insights into the design of the four hand-crafted features used in our R@1 predictor (described in Section III-C of the main manuscript). To reiterate once more, these were the four features used in this work with significant performance results across methods and datasets: it is, of course, likely that a much larger set of features is viable, and that more systematic methods of discovering these features would lead to further performance improvements.

Our feature design was guided by qualitatively analysing the VPR matching behaviour. We examined prediction score distributions and visualised qualitative examples of correct and incorrect matches across varying difficulty conditions. By inspecting the top-1 retrieved candidates and their associated distance scores, we identified recurring spatial patterns that

distinguish reliable matches from unreliable ones. We explain the intuition behind each feature and why they effectively capture spatial matching quality.

1) *Jump rate:  $(x_{i,k,1})$*  When VPR matching is reliable, consecutive query images (captured along a continuous trajectory) should match to spatially proximate reference images. Large spatial discontinuities between consecutive predictions indicate false VPR matches. This feature is a measure of how frequently predictions “jump” beyond the ground-truth tolerance threshold.

2) *Fraction Outside Main Cluster:  $(x_{i,k,2})$*  In segments where all query predictions are correct, the predictions should concentrate within a spatially coherent region corresponding to the true places. This feature quantifies spatial dispersion by measuring what fraction of predictions fall outside the dominant spatial region and its immediate neighbours. A high value means that the predictions are distributed across multiple unrelated regions, signalling low matching confidence.

3) *Largest Cluster Fraction:  $(x_{i,k,3})$*  Unlike the  $x_{i,k,2}$  feature, which penalises dispersion, this complementary feature rewards concentration, where a high value indicates that most predictions are within the same region. This feature distinguishes between segments with one dominant coherent region and those with spatially-fragmented predictions.

4) *Turn Rate:  $(x_{i,k,4})$*  For a vehicle or robot traversing a route, the sequence of matched reference positions should follow a generally monotonic pattern (e.g., increasing along a reference traversal). This feature captures frequent reversals in the matched reference positions through the non-zero second order differences. If the matched reference places for continuous queries oscillate between different geographically-distant places, it indicates that the query predictions for a segment have high matching ambiguity.

#### B. Distribution of RAR deviations across VPR models and datasets

Table I of the main manuscript demonstrates that our approach reliably meets or exceeds the target RAR thresholds across varying target R@1 and target RAR thresholds for the evaluated VPR models and datasets. Figure S1 presents the distribution of the RAR deviations between the achieved and achievable RAR in histogram form to provide a more detailed view of the performance across all operating conditions.

Our approach very consistently achieves non-negative deviations (with no exceptions): all bars fall on or to the right of the zero line across both datasets and VPR models. This confirms that our adaptive sampling strategy reliably satisfies the target RAR constraints. The static baseline (SR4:  $k = 4$ ) shows dataset-dependent behaviour. On Oxford RobotCar (fig. S1c,d), it performs comparably to our approach, with most deviations at or above zero. However, on Nordland (fig. S1a,b), the baseline fails substantially, with deviations as low as

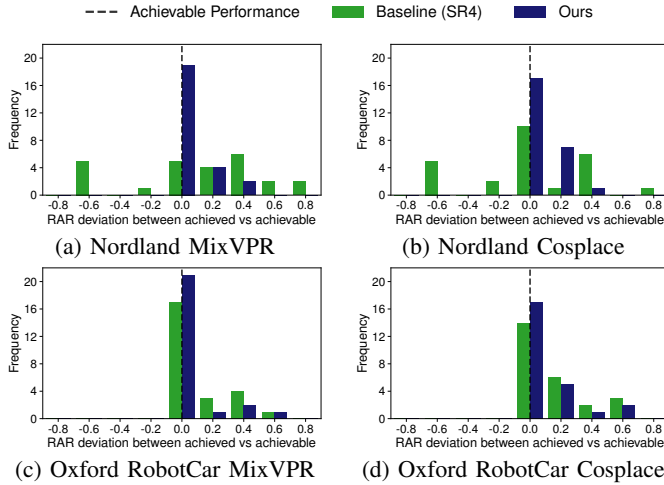


Fig. S1: Distribution of RAR deviation between the achieved and achievable RAR across all target R@1 and target RAR conditions for each VPR model and dataset combination. Our approach (navy) consistently achieves non-negative deviations, while the static baseline (green, SR4:  $k = 4$ ) fails substantially on Nordland despite succeeding on Oxford RobotCar.

−0.64. This discrepancy arises because a fixed sampling rate cannot adapt to user-specified per-segment target R@1 and target RAR requirements for the Nordland dataset which might have greater spatial variability in matching difficulty compared to the Oxford RobotCar dataset. In contrast, our approach maintains consistent performance across both datasets, demonstrating its robustness to varying environmental conditions.

### C. The recall achievement rate (RAR) and reference density trade-offs

Section V-A of the main manuscript demonstrated that our approach reliably meets or exceeds user-specified target recall achievement rate (RAR) thresholds. This section provides a detailed analysis of the relationship between reference density, RAR, and our method’s selection behaviour using MixVPR on Nordland.

1) *Varying Target RAR at Fixed Target R@1*: Figure S2 presents RAR against the total number of reference images for each sampling rate (grey curve), with a fixed per-segment target R@1 of 80% and varying target RAR thresholds (20%–100%). The red dashed line indicates the target RAR, the yellow square marks the oracle (the sparsest sampling rate meeting the target), and the blue star marks the selected reference density of our approach.

Two key observations emerge. First, our method consistently meets or exceeds the target RAR across all conditions, with the selected sampling rate always falling on or above the red threshold line. Second, for most conditions, multiple sampling rates satisfy the target RAR constraint; our method reliably identifies the sparsest acceptable option, often matching or closely approximating the oracle. Note that the grey curve remains identical across all subplots since the achievable RAR

at each sampling rate depends only on the per-segment target R@1, which is held constant here.

2) *Varying Target R@1 at Fixed Target RAR*: Figure S3 examines the complementary scenario where the target RAR (60%) is fixed while varying the per-segment target R@1 thresholds (20%–100%). In contrast to Figure S2, the grey curve now changes across subplots, reflecting how the achievable RAR at each sampling rate depends on the target R@1 threshold.

As the target R@1 increases, achieving high RAR becomes progressively more difficult for sparser sampling rates. This is evident in the rightward shift of the grey curve. For example, at target R@1 = 20% (fig. S3a), even sparse sampling rates achieve high RAR, whereas at target R@1 = 100% (fig. S3e), only the densest sampling rate meets the threshold. Despite this increasing difficulty, our method adapts appropriately, selecting sparser densities when feasible and denser densities only when necessary to satisfy the target constraint.

These results show that our method navigates the RAR and reference density trade-off effectively, as it exploits opportunities to reduce reference storage when conditions permit while ensuring that the target constraints are satisfied.

### D. Global mean recall can mask local recall variability

In Section V-C of the main manuscript, we demonstrated that a high mean R@1 does not guarantee a high RAR for a given per-segment target R@1. Figure S4 extends this analysis to additional VPR methods and datasets: CosPlace on Nordland, MixVPR on Oxford RobotCar, and CosPlace on Oxford RobotCar.

1) *Key observations across all configurations*: Consistent with the main manuscript, the extended results confirm two fundamental properties of RAR. First, RAR is dependent on the per-segment target R@1 threshold, whereas mean R@1 remains constant regardless of the threshold chosen. Second, as the per-segment target R@1 increases, the RAR for each sampling density shifts leftward, reflecting the fact that fewer segments can satisfy stricter local recall requirements.

2) *Nordland dataset analysis*: The Nordland results (fig. S4a) illustrate how dramatically RAR varies with the per-segment target R@1, whilst the mean R@1 remains unchanged. Consider the sampling rate SR10 ( $k=10$ ) evaluated with CosPlace: while its mean R@1 remains constant at 61%, its RAR decreases substantially as the target threshold increases: from a RAR of 99% at a 20% target threshold to 0% at a 100% target threshold, passing through 95%, 54%, and 11% at thresholds of 40%, 60%, and 80%, respectively. This example shows that a single sampling rate can have vastly different local performance achievements, information that the mean R@1 alone cannot reveal.

Furthermore, at the strictest threshold (per-segment target R@1 of 100%), only the two densest sampling rates, SR1 (RAR = 56%) and SR2 (RAR = 5%), achieve non-zero RAR values. All sparser sampling rates fail to produce any segments with perfect local recall. Notably, the mean R@1 values for SR1, SR2, and SR3 are 97%, 93%, and 89%,

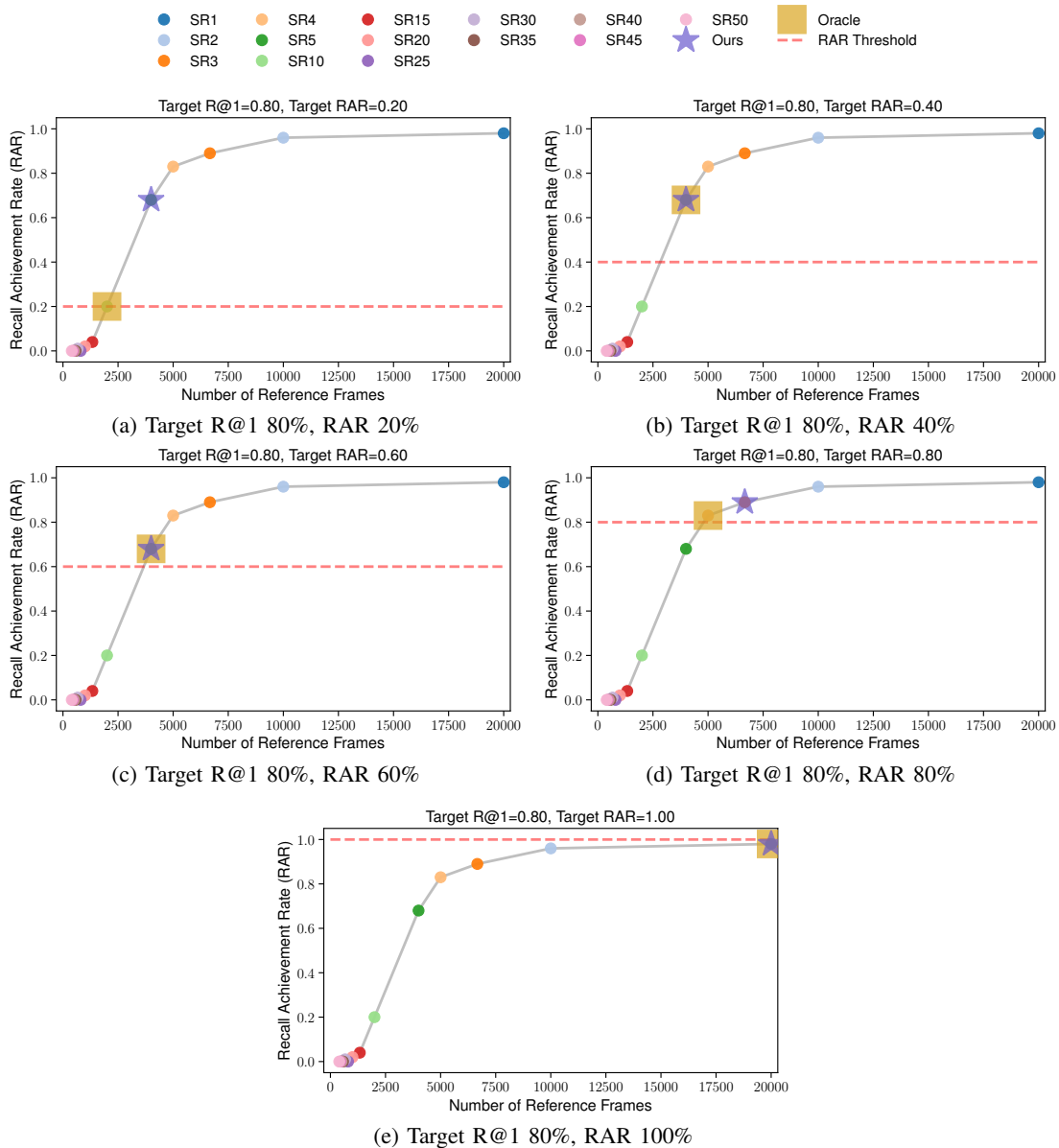


Fig. S2: **Fixed target R@1, varying target RAR thresholds.** RAR versus number of reference images for each sampling rate (grey curve) using MixVPR on Nordland, with per-segment target R@1 fixed at 80% and target RAR varying from 20% to 100% (a–e). The grey curve remains identical across subplots since achievable RAR depends only on target R@1. Blue star: our method’s selection; yellow square: oracle (sparsest sampling rate meeting the target); red dashed line: target RAR threshold. Our approach meets or exceeds the target RAR in all cases, selecting the sparsest acceptable sampling rate.

respectively, which are values that appear similar but mask the stark differences in local performance consistency. This shows that the mean R@1 cannot capture the spatial distribution of matching performance, whereas RAR provides a measure of how consistently a target recall is achieved across segments.

3) *Oxford RobotCar dataset analysis:* The Oxford RobotCar results (fig. S4b,c) show a more compressed vertical range compared to Nordland, with mean R@1 values concentrated between 0.75 and 1.00. This reflects both the lower difficulty of the Oxford RobotCar environment and the permissive ground-truth tolerance ( $\pm 25m$ ), which together enable most sampling rates to achieve high recall. We selected a relatively

high ground truth tolerance to ensure that every query image has at least one matching reference place.

Despite this compressed range, the dependence of the RAR on per-segment target R@1 is evident. At lower per-segment target R@1 thresholds (20% and 40%), the RAR for all sampling rates clusters between 95% and 100% for both MixVPR and CosPlace. At a target R@1 of 60%, RAR remains high across all sampling rates for MixVPR, but begins to decline more noticeably for CosPlace. At higher thresholds (80% and 100%), the decline in RAR becomes increasingly pronounced, particularly for sparser sampling densities.

For example, for CosPlace on Oxford RobotCar, the sam-

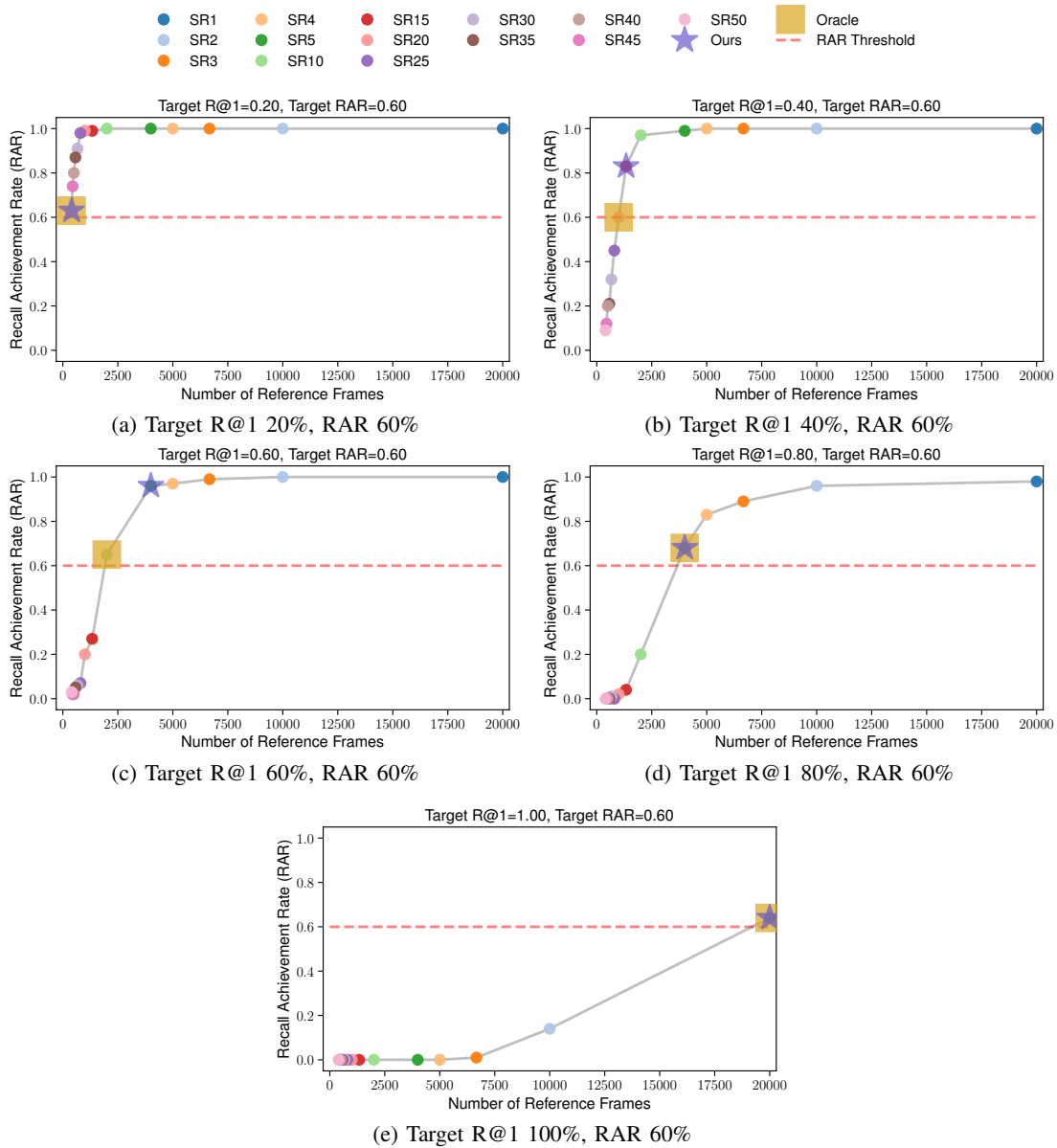


Fig. S3: **Fixed target RAR, varying target R@1 thresholds.** RAR versus number of reference images for each sampling rate (grey curve) using MixVPR on Nordland, with target RAR fixed at 60% and per-segment target R@1 varying from 20% to 100% (a–e). The grey curve shifts rightward as target R@1 increases, reflecting the greater difficulty of achieving high RAR under stricter recall requirements. Blue star: our method’s selection; yellow square: oracle; red dashed line: target RAR threshold. Our approach adapts to varying difficulty, meeting or exceeding the target in all cases.

pling density of 35 (SR35:  $k = 35$ ) achieves a mean R@1 of 92%. Its RAR remains above 95% for per-segment target R@1 thresholds of 20%, 40%, and 60%. However, at thresholds of 80% and 100%, its RAR drops to 84% and 41%, respectively. In other words, although SR35 achieves a 92% mean recall globally, only 84% of segments exceed 80% local recall, and only 41% of segments achieve perfect local recall. This disparity highlights that comparable mean R@1 values can correspond to substantially different levels of spatial consistency in performance, which is a distinction that is critical for deployment scenarios requiring local performance guarantees.

#### E. Ablation study on swapping the roles of the two reference sets

This section expands on the ablation study discussed in Section IV-D of the main text, providing additional results and analysis.

We swapped the roles of the two reference sets during Phase 1 to test whether our approach’s performance depends on which specific reference traverse is used for training. In the original configuration, predictors are trained on (Ref1, Ref2) and evaluated on (Ref1\*, Qry1); in the swapped configuration, training uses (Ref2, Ref1) and evaluation uses (Ref2\*, Qry1).

Figure S5 presents heatmaps of deviations from the target

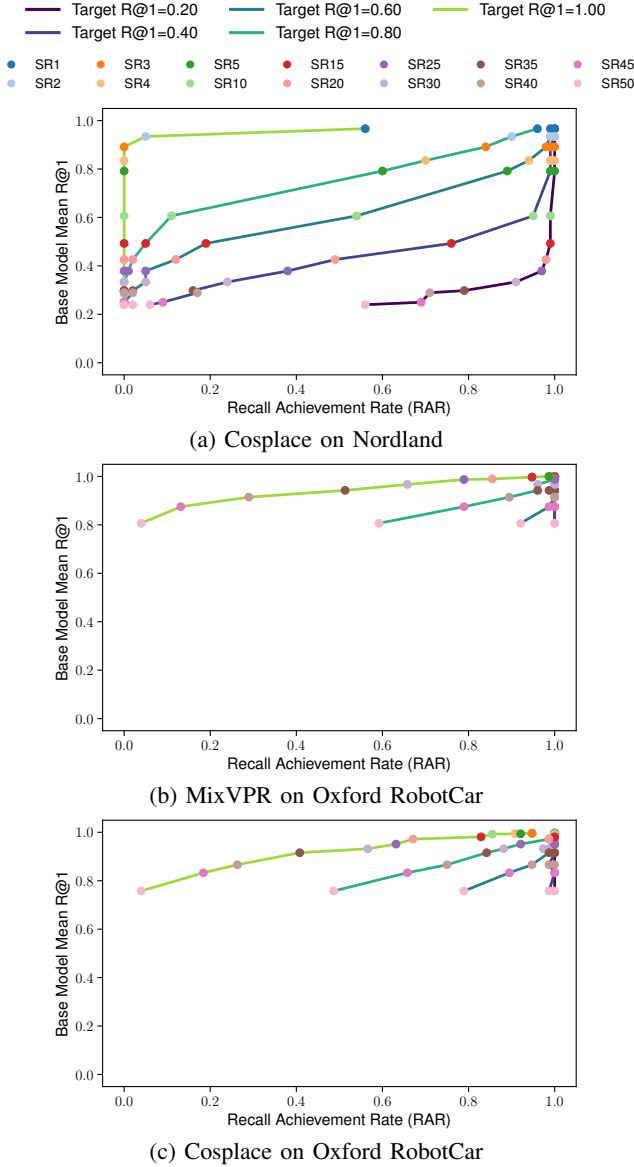


Fig. S4: The recall achievement rate (RAR) of the different sampling rates against the mean R@1 for different per-segment target R@1 of 20%, 40%, 60%, 80% and 100%. Observations: the RAR metric is dependent on the per-segment target R@1 whereas the global mean R@1 is not. With increasing per-segment target R@1, the point for the same sampling density is pushed leftward, as less segments meet that stricter target R@1.

RAR for the original configuration (left), the swapped configuration (middle), and their difference (right). The majority of conditions show zero or negligible differences, indicating the robustness of our method to reference traversal selection. The largest deviations occur at target R@1 values (20% and 80%), where the swapped configuration increases RAR by up to 0.24. All other conditions remain consistent, demonstrating that our method learns generalisable spatial matching characteristics.

#### F. Ablation study on the impact of changing the segment length

This section expands on the segment length ablation study discussed in Section IV-E of the main text, providing detailed results across all tested configurations. Figure S6 presents heatmaps showing the deviation from target RAR for segment lengths ranging from 50m to 300m (in 50m increments) across all target R@1 and RAR threshold combinations.

All segment lengths achieve perfect target matching (deviation = 0.00) for the majority of operating conditions, particularly in the mid-range of target R@1 (40%-60%) and higher RAR thresholds (60–100%).

At shorter segment lengths (50-100m), our approach obtains larger positive deviations under some conditions (target R@1 = 100%, low RAR thresholds), achieving up to 0.61 above the target. This over-achievement suggests that fine-grained segments may capture highly localised variations that lead to conservative density selection. The segment length of 100 m shows a minor under-achievement (negative deviation of -0.16) under the condition (target R@1 = 60%, target RAR = 20%). However, this deviation is partially an artifact of the discrete sampling density options: the selected density (SR20:  $k = 20$ ) achieves a RAR of 18%, only 2% below target, while the next sparsest acceptable density (SR15:  $k = 15$ ) achieves 34%, which is 14% above target. Since deviation is computed against the nearest achievable density, the reported error overstates the practical shortfall.

The longer segment lengths (250-300 m) show more conservative and stable performance with smaller deviations, achieving near-zero deviation across more conditions compared to shorter segments. However, they show slight under-achievement (negative deviations up to -0.11) under the condition (target R@1 = 20%, target RAR = 80%). At longer segment lengths, localised difficult regions may be masked by easier regions, causing the predictor to overestimate per-segment R@1 and consequently select overly sparse sampling densities.

The segment lengths of 150-200 m provide stable performance across most conditions, with sufficient capability to adapt to local variations. These configurations maintain consistent performance across most conditions while retaining sufficient granularity to capture local spatial variations in matching difficulty.

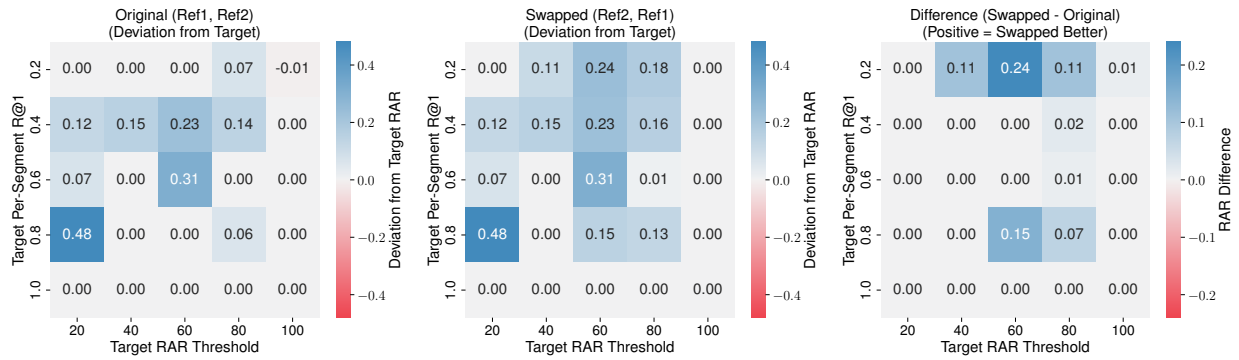


Fig. S5: Ablation study on swapping Ref1 and Ref2: Comparison of RAR deviations between achieved and achievable RAR for original configuration (Ref1, Ref2) (left), swapped configuration (Ref2, Ref1) (middle), and their difference (right), showing the effect of reference role swap across different configurations.

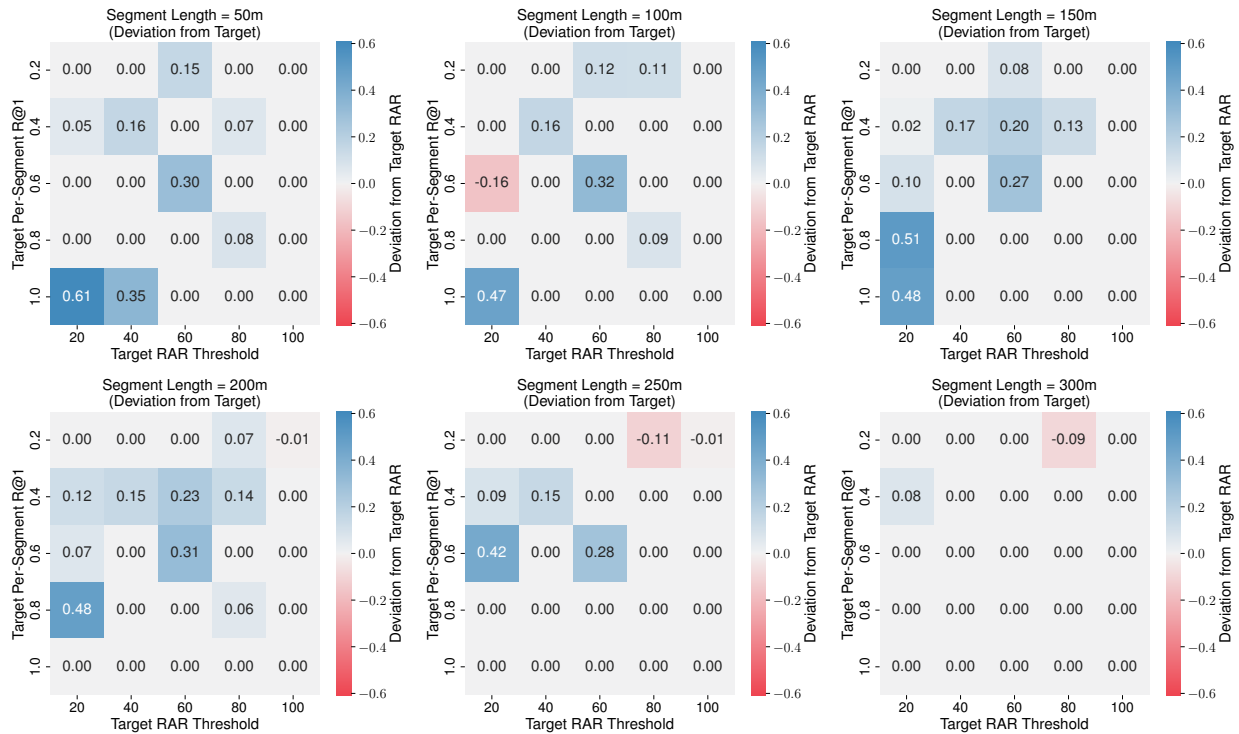


Fig. S6: Ablation study on the impact of changing the segment length: The impact of segment length on RAR achievement across different target operating conditions. Each heatmap shows the RAR deviation from between achieved and achievable RAR for a specific segment length (50m to 300m).